Fundamental Carrier Lifetime Exceeding 1 µs in Cs$_2$AgBiBr$_6$ Double Perovskite

Robert L. Z. Hoye,* Lissa Eyre, Fengxia Wei, Federico Brivio, Aditya Sadhanala, Shijing Sun, Weiwei Li, Kelvin H. L. Zhang, Judith L. MacManus-Driscoll, Paul D. Bristowe, Richard H. Friend,* Anthony K. Cheetham,* and Felix Deschler*

There is current interest in finding nontoxic alternatives to lead-halide perovskites for optoelectronic applications. Silver–bismuth double perovskites have recently gained attention, but evaluating their carrier lifetime and recombination mechanisms from photoluminescence measurements is challenging due to their indirect bandgap. In this work, transient absorption spectroscopy is used to directly track the photocarrier population in Cs$_2$AgBiBr$_6$ by measuring the ground state bleach dynamics. A small initial drop is resolved in the ground state bleach on a picosecond timescale, after which the remaining photocarriers decay monoexponentially with a lifetime of 1.4 µs. The majority of the early-time decay is attributed to hot-carrier thermalization from the direct transition to the indirect bandgap, and the 1.4 µs lifetime represents the recombination of most photocarriers. From this lifetime, a steady-state excess carrier density of 2.2×10^{16} cm^{-3} under 1 sun is calculated, which is an order of magnitude larger than that for methylammonium lead iodide, suggesting that charge transport and extraction can be efficient in Cs$_2$AgBiBr$_6$ solar cells.

Lead-halide perovskites display remarkable optoelectronic properties, with long diffusion lengths >1 µm,[1,2] strong optical absorption on the order of 10^5 cm^{-1},[3] and high photoluminescence quantum efficiencies >80%.[4] These properties have led to rapid increases in the efficiency of perovskite solar cells (up to a certified power conversion efficiency of 22.7%)[5] and light emitting diodes (>11% external quantum efficiency)[6] over a short period of time. However, the toxicity of the lead content and limited air-stability of some compositions has motivated researchers to find lead-free alternatives.[7,8] A wide range of materials classes have recently been explored computationally and experimentally.[8,9] In evaluating the potential of these new materials for photovoltaics, much of the focus has been on the bandgap, stability, absorption coefficient, and phase.[8,10–13] The minority-carrier lifetime has received less attention, yet has historically limited the development of new photovoltaic materials.[14,15] However, the reported lifetimes of lead-free alternatives to the perovskites have typically ranged from <0.1 to ≈10 ns.[15–17] Silver–bismuth double perovskites (e.g., Cs$_2$AgBiBr$_6$ and Cs$_2$AgBiCl$_6$) have recently been found to be an exception. Time-resolved photoluminescence (TRPL) measurements of these materials show an initial drop in photoluminescence (PL) over a nanosecond timescale by 0.5–2 orders of magnitude, followed by a slow tail in PL decay. These PL decay traces are fit with a bi- or triexponential model and the longest time constant is attributed to the fundamental lifetime, which has been found to be ≥100 ns.[18–20] Given that these materials have also been found to be more stable than methylammonium lead iodide,[18,20] they have attracted significant interest, with many recent investigations of new families of double perovskite compounds with novel properties.

Dr. R. L. Z. Hoye, L. Eyre, Dr. A. Sadhanala, Prof. R. H. Friend, Dr. F. Deschler
Cavendish Laboratory
JJ Thomson Ave
University of Cambridge
Cambridge CB3 0HE, UK
E-mail: rlzh2@cam.ac.uk; rhf10@cam.ac.uk; fd297@cam.ac.uk

Dr. F. Wei, Dr. F. Brivio, Dr. S. Sun, Dr. W. Li, Prof. K. H. L. Zhang, Prof. J. L. MacManus-Driscoll, Dr. P. D. Bristowe, Prof. A. K. Cheetham
Department of Materials Science and Metallurgy
University of Cambridge
27 Charles Babbage Rd, Cambridge CB3 0FS, UK
E-mail: akc30@cam.ac.uk

Dr. F. Wei
Institute of Materials Research and Engineering
Agency for Science
Technology and Research
2 Fusionopolis Way, Singapore 138634, Singapore

Dr. S. Sun
Massachusetts Institute of Technology
Cambridge, MA 02139, USA

Prof. K. H. L. Zhang
College of Chemistry and Chemical Engineering
Xiamen University
Xiamen 361005, P. R. China

Double perovskites have the general formula: $A_2M^IM^{III}X_6$, where A and M^I are monovalent cations, M^{III} a trivalent cation and X a halide.[21] The Pb^{2+} in lead–halide perovskites can therefore be substituted for more benign monovalent (e.g., Ag^+) and trivalent cations (e.g., Bi^{3+}), while maintaining a 3D perovskite crystallographic structure.[22] Recently, Greul et al. reported the first $Cs_2AgBiBr_6$ solar cell, with high external quantum efficiencies reaching 60%.[23] However, it is unknown whether the steady-state excess carrier density could support efficient transport in thicker absorbers, which will be important for increasing the light absorption in the indirect-bandgap material. Although reasonable mobilities of 1 cm^2 V^{-1} s^{-1} (thin films) and 3–12 cm^2 V^{-1} s^{-1} (single crystals) have been reported,[24,25] the large initial drop in PL may limit the achievable steady-state carrier densities. Furthermore, the PL emission energy reported in $Cs_2AgBiBr_6$ is often below the measured optical bandgap and weak. This prompts questions on how accurately the PL tracks the decay of photocarriers across the band-edges, and whether the PL lifetimes reported represent the recombination of most photogenerated excess carriers. Recent time-resolved microwave conductance measurements have also shown a large initial drop in signal, particularly in thin films, which was attributed to surface recombination.[25] In this work, we perform detailed spectroscopy and ultrafast dynamic measurements on $Cs_2AgBiBr_6$ single crystals and thin films, with comparison to

$Cs_2AgBiCl_6$ single crystals. We seek to understand the mechanism of PL decay and what it represents, and to determine the 1 sun excess carrier density by directly measuring the recombination of all photocarriers across the indirect bandgap.

Single crystals of $Cs_2AgBiBr_6$ and $Cs_2AgBiCl_6$ were grown by slow precipitation at low temperature from a saturated solution (refer to the Experimental Section). The absorbance of the single crystals was measured by photothermal deflection spectroscopy (PDS), which gives a more accurate measure of the sub-bandgap absorbance than reflectance measurements in UV–vis spectrophotometry and is important for us to analyze the defects in our crystals. The optical gaps from the Tauc plots were found to be 2.0 eV for $Cs_2AgBiBr_6$ and 2.5 eV for $Cs_2AgBiCl_6$ (**Figure 1**a,b). Both materials have significant absorbance extending below their absorption edges (Figure 1c,d). The PL peaks for both double perovskites were centered below the optical bandgaps, broad and asymmetric.

These observations are consistent with the presence of sub-bandgap defect states that are involved in emissive recombination. The low absorption edge slopes in the PDS spectra (dashed yellow lines) indicate high levels of disorder, with an Urbach energy of 170 meV for $Cs_2AgBiBr_6$ and 95 meV for $Cs_2AgBiCl_6$. These may be due to Ag_{Bi} antisite defects, or Ag or Cs vacancies.[26] Our results are consistent with observations that annealing $Cs_2AgBiBr_6$ single crystals to reduce the trap
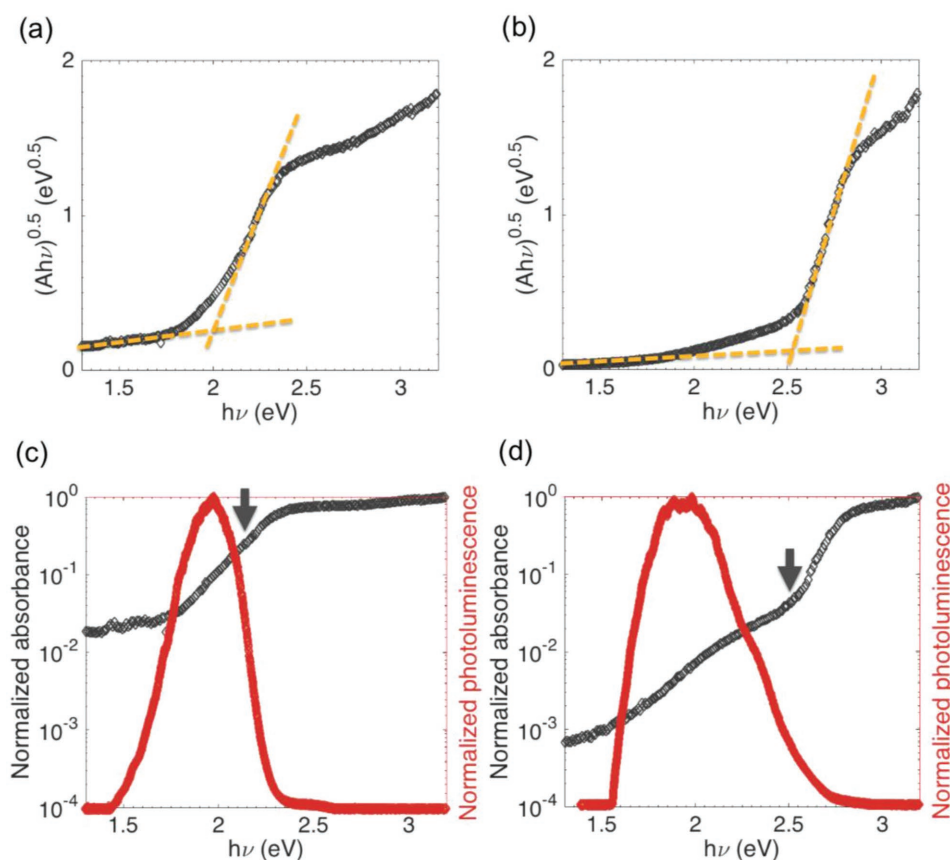
Figure 1. Tauc plots for a) $Cs_2AgBiBr_6$ and b) $Cs_2AgBiCl_6$ single crystals. The normalized absorbance (A) measured by photothermal deflection spectroscopy is used for the $(Ah\nu)^{0.5}$ term on the vertical axis. Comparison of the normalized absorbance and spectrally resolved photoluminescence of c) $Cs_2AgBiBr_6$ and d) $Cs_2AgBiCl_6$ single crystals on semilogarithmic axes. Arrows indicate onset of main absorption.

**Table 1.** Optical properties of $Cs_2AgBiBr_6$ and $Cs_2AgBiCl_6$.

Material	Reported E_g [eV]	Measured E_g [eV]	PL peak [eV]
$Cs_2AgBiBr_6$	1.95–2.19[10,18,28]	2.0	1.95
$Cs_2AgBiCl_6$	2.77[28]	2.5	1.90

density leads to a blue-shift in the photoluminescence closer to the optical gap.[24] We note that sub-bandgap absorption in our Cs_2AgBiX_6 materials could also be due to phonon absorption and emission. But as detailed in Figures S1 and S2 in the Supporting Information, the phonon energies that would account for this (170 meV for $Cs_2AgBiBr_6$, 380 meV for $Cs_2AgBiCl_6$) are an order of magnitude larger than predicted, in agreement with observations by Filip et al.[27] We therefore believe it more likely that the sub-bandgap PL is due to defect emission. In particular, we note that although $Cs_2AgBiCl_6$ has a wider optical bandgap than $Cs_2AgBiBr_6$, the PL is centered at a similar energy (1.90 cf. 1.95 eV, **Table 1**) and coincides with the shoulder in sub-bandgap absorbance (Figure 1d), which supports PL originating from recombination to defects.

To compare the TRPL traces of both crystals, we measured the transient PL spectra using an intensified charge-coupled device (ICCD) camera (**Figure 2**), which provided time and spectral resolution. We note that our ICCD camera had a time-resolution of 4 ns and we measured photoluminescence

from radiative recombination events occurring >1 ns after excitation. The TRPL traces of our single crystals were fluence-independent (Figures S3 and S4, Supporting Information). Furthermore, when we shifted time zero so that the maximum PL matched the PL value from the trace for the next highest fluence, we found that the traces were not overlaid. This suggests that more than one recombination process occurred. The TRPL traces of both crystals exhibited an initial fast decay (over tens of nanoseconds) followed by a slower tail, consistent with previous observations.[18,20]

However, the PL emission of both single crystal materials was weak and required high fluences to observe. To quantify the photoluminescence quantum efficiency (PLQE), we measured the samples inside an integrating sphere. Our $Cs_2AgBiCl_6$ single crystals had large flat faces, to which we could align the excitation laser (at 405 nm). We measured a PLQE of 7% at 500 mW cm^{-2} and 2.6% at a 1500 mW cm^{-2} power density. The $Cs_2AgBiBr_6$ single crystals were too small for this measurement. We therefore synthesized thin films following a recently reported method,[19] achieving the highest phase-purity (99.75% $Cs_2AgBiBr_6$; Figures S5 and S6, Supporting Information) with 5 min annealing at 250 °C inside a nitrogen-filled glovebox. The optimized thin films had a lower Urbach energy than the $Cs_2AgBiBr_6$ single crystal, and also a low sub-bandgap absorption coefficient (Figure S7, Supporting Information). The PL emission of the $Cs_2AgBiBr_6$ thin film (**Figure 3**a) was at the
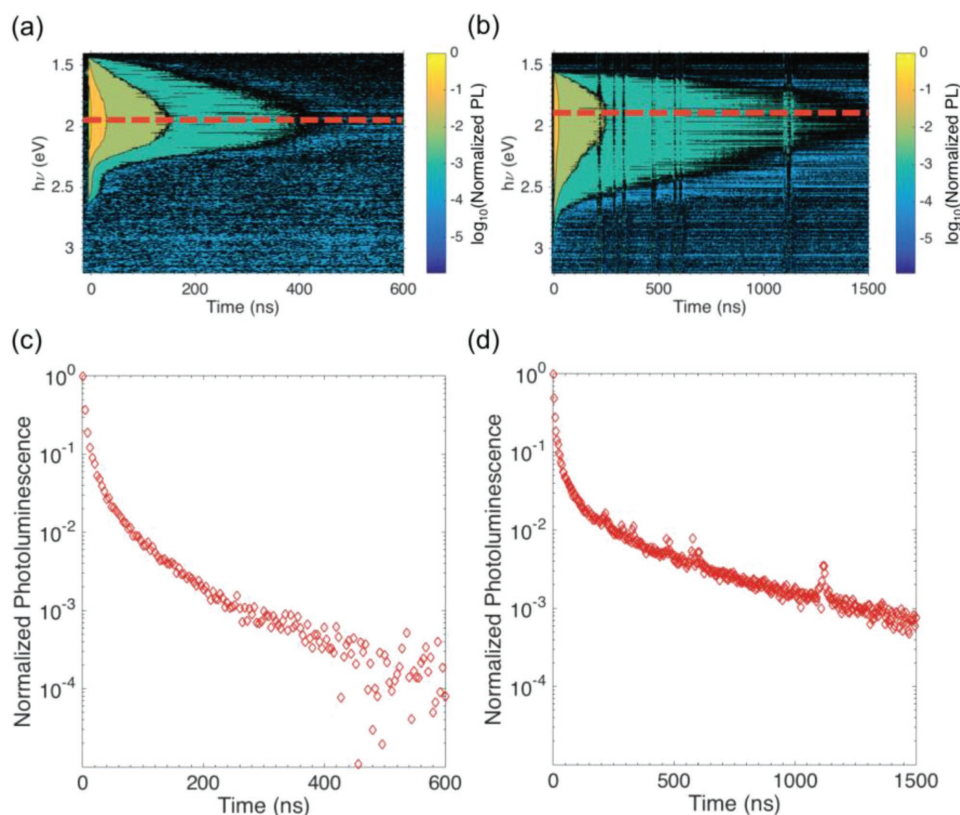
Figure 2. Time resolved photoluminescence measurements of single crystals of a) $Cs_2AgBiBr_6$ and b) $Cs_2AgBiCl_6$. Normalized photoluminescence (PL) decays at emission energies corresponding to the peak PL intensity of c) $Cs_2AgBiBr_6$ and d) $Cs_2AgBiCl_6$. The excitation wavelength was 400 nm, laser pulse length 100 fs and repetition rate 1 kHz. For the data shown, the fluences used were 150–160 μJ cm^{-2} pulse^{-1}. The fluence-dependent data are shown in Figures S3 and S4 in the Supporting Information.
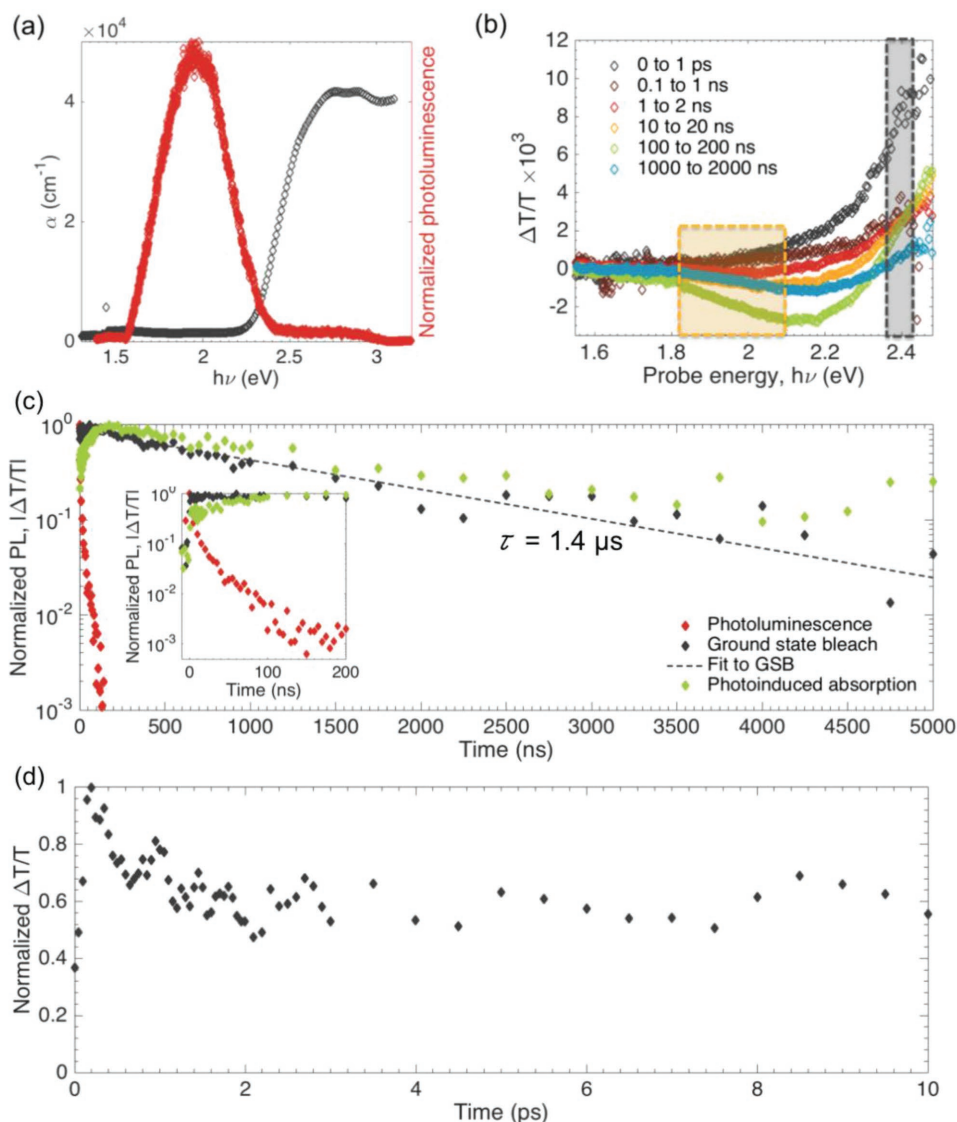
Figure 3. Optical measurements of the same $Cs_2AgBiBr_6$ film with a thickness of 520 ± 40 nm. a) Absorption coefficient and photoluminescence (PL) measurements. Bandgap analysis is in Figure S7 in the Supporting Information. b) $\Delta T/T$ spectra at different time ranges. c) Normalized kinetics of the ground state bleach (GSB) and photoinduced absorption compared to the normalized PL decay. The excitation wavelength was 355 nm and fluence 90–120 μJ cm^{-2} pulse^{-1}. The $\Delta T/T$ values were integrated from the spectra in inset (b) (gray range for GSB; yellow range for photoinduced absorption). The GSB decay was fit with a monoexponential function, and the time constant was 1.4 μs. Inset is a zoom-in of the kinetics between 0 and 200 ns. d) Normalized short-time $\Delta T/T$ kinetics on picosecond timescales. The excitation wavelength was 400 nm for laser pulses with a pulse length of 100 fs at a repetition rate of 1 kHz and fluence of 10 μJ cm^{-2} pulse^{-1}. The GSB signal was integrated over the gray shaded spectral range shown in inset (b).

same energy as the single crystals and comparably weak. At a power density of 500 mW cm^{-2}, the PLQE was 0.01% and at 1500 mW cm^{-2} was 0.02%. TRPL of these double perovskites therefore only measures the decay of a small fraction of carriers, which may be filling traps rather than directly recombining across the indirect bandgap. These results suggest that there are potential parallel recombination processes for the vast majority of the carriers, which are not measured by TRPL.

In order to measure the kinetics of all photocarriers, we performed transient absorption spectroscopy. Transient absorption is a pump-probe technique that measures the population of carriers after excitation $t = 0$ ns. For these measurements, we focused on our $Cs_2AgBiBr_6$ thin films, which we could measure

in transmission. Measuring thin films in transmission is more accurate than measuring single crystals because we avoid artifacts due to nonuniform scattering of the pump and probe beams.

The transient absorption spectra of our $Cs_2AgBiBr_6$ thin film are shown in Figure 3b at different times after excitation. The short-time (200 fs–1 ns) and long-time (>1 ns) spectra were measured using different pump sources (detailed in the Experimental Section). A ground state bleach (i.e., positive value of $\Delta T/T$) was observed for energies $\geq$2.3 eV for all spectra. The ground state bleach corresponds to a population of electrons excited across the bandgap. We note than an energy of 2.3 eV is higher than the optical bandgap, which we estimated to be

between 2.05 and 2.2 eV based on analyses of the absorption coefficient of our thin film (Figure S7, Supporting Information). The number of states at the indirect band-edge of our thin film may be insufficient to produce a measurable $\Delta T/T$. However, we would expect the dynamics measured slightly above the band-edge to be similar or faster than band-edge recombination, since hot carriers may thermalize to the band-edge as well as recombine.

We integrated the ground state bleach between 2.36 and 2.43 eV for the long-time measurements, and found the kinetics to be fluence-independent (Figure S10, Supporting Information), decaying monoexponentially with a time-constant of 1.4 μs, two orders of magnitude slower than the PL decay (Figure 3c). In our transient absorption spectra, we also observed a photoinduced absorption (negative $\Delta T/T$) centered at 2.14 eV (Figure 3b). The photoinduced absorption in $Cs_2AgBiBr_6$ decayed on a similar timescale as the ground state bleach (Figure 3c), which further supports the slow decay of photocarriers on a microsecond timescale, since photoinduced absorption can only arise from states produced after excitation.

Short-time transient absorption spectroscopy gave us further insight into the photocarrier dynamics. These measurements are shown in Figure 3d. We observed an initial circa 50% reduction in the ground state bleach signal over the first picosecond, followed by a further fluence-dependent reduction in ground state bleach over the next nanosecond. Two possible origins for this decay in ground state bleach are 1) thermalization of hot carriers to the band-extrema, and 2) nonradiative recombination via surface or bulk defects. In the case of indirect-bandgap materials, thermalization involves not only hot carrier relaxation at the direct transition, but also relaxation across k-space to the indirect bandgap. If all excited electrons thermalized to the band-edge, we would expect the ground state bleach at 2.3 eV to decrease by 50%, which would match the measured initial drop in ground state bleach. Hot-carrier thermalization does not represent a limitation in photovoltaic potential. But the second case would represent a loss in carriers and the defects responsible would need to be passivated to achieve high photovoltaic performance. However, it is unlikely that recombination at surface defects would result in the picosecond drop in carrier population, since the diffusivity of carriers to the surface would need to be at least an order of magnitude larger than is achievable with the reported mobilities in $Cs_2AgBiBr_6$. We note that in the long-time transient absorption measurements, there was no rapid early-time decrease in ground state bleach. The long-time measurements used longer pulses, such that the peak photon flux density in each pulse was lower for the same fluence than the short-time measurements. In Figure S10 in the Supporting Information it can be seen that the short-time kinetics were slower at lower fluences and more closely matched with the long-time measurements. Therefore, in comparing the short- and long-time measurements, it is most appropriate to use the short-time measurements made under the lowest fluence of 10 μJ cm^{-2} pulse^{-1} because that is when the peak instantaneous photon fluxes are most similar. The picosecond drop in ground state bleach in the short-time measurements may not be detected in the long-time measurements due to jitter in the timing electronics. Long-time measurements therefore track the dynamics of photocarriers present >1 ns after excitation.

We note that the TRPL measurements were performed on the same timescale as the long-time transient absorption measurements (i.e., >1 ns after excitation). The sharp difference between the TRPL and transient absorption measurements is likely due to PL originating from a different recombination mechanism than that mainly responsible for the slow decay of the ground state bleach. Whereas photocarriers present >1 ns after excitation primarily slowly recombine nonradiatively across the indirect bandgap, radiative recombination may be more likely to occur via defects. This is because defects produce states that are delocalized across k-space, thereby requiring a smaller phonon contribution for electronic transitions. We also observed that the PL decay time in our $Cs_2AgBiBr_6$ thin film agrees with the rise in photoinduced absorption (Figure 3c, right). The data suggests that the process of radiative recombination fills previously unoccupied states, which then give rise to the photoinduced absorption that decays with almost identical kinetics as the ground state bleach (Figure 3c).

In addition to evidence for these defect states in $Cs_2AgBiBr_6$ from our PDS measurements (discussed earlier), our X-ray photoemission spectra also provide support (**Figure 4**a). We fitted the valence spectrum of our $Cs_2AgBiBr_6$ thin film with the density of states reported by McClure et al.[28] using a previously reported method.[8] From this, we found the valence band maximum to be 0.1 eV below the Fermi level, indicating the material to be p-type. This would occur if acceptor defects are present (e.g., Ag_{Bi} antisites, Ag vacancies, or Cs vacancies), as
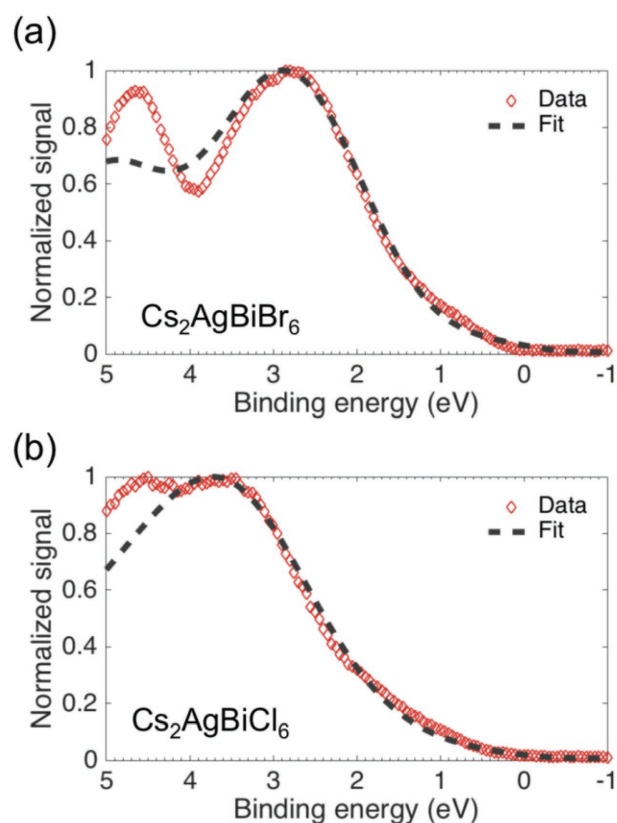
Figure 4. Valence band X-ray photoemission spectra of a) $Cs_2AgBiBr_6$ thin film and b) $Cs_2AgBiCl_6$ single crystal.

**ADVANCED
SCIENCE NEWS**
www.advancedsciencenews.com

**ADVANCED
MATERIALS
INTERFACES**
www.advmatinterfaces.de

predicted by theory.[26] We also note that from fitting the valence band spectrum of $Cs_2AgBiCl_6$, the material is also p-type, with a valence band maximum 0.4 eV below the Fermi level (Figure 4b). This, with the PDS measurements, is in agreement with the presence of acceptor defects close to the valence band maximum, and we would also expect the PL decay in $Cs_2AgBiCl_6$ to arise from a different mechanism to the recombination of most photocarriers.

We note that the long-lived photocarriers measured in our $Cs_2AgBiBr_6$ thin film may also relax to a trap state and be thermally re-excited to the band-edge, as was proposed in a recent investigation using time-resolved microwave conductance at different temperatures.[25] This recent investigation also estimated the lower bound of the mobility to be 1 $cm^2 V^{-1} s^{-1}$, suggesting the long-lived carriers to be mobile.[25] If these trapping and detrapping processes are present, we would expect the ground state bleach to decay while the photoinduced absorption rises, which is not the case (Figure 3c), but this may be due to trapping/detrapping occurring rapidly. The equal rate of decay in the photoinduced absorption and ground state bleach suggests that these slow processes are due to carrier recombination across the bandgap.

A long fundamental lifetime of photocarriers is consistent with the high external quantum efficiencies reported for $Cs_2AgBiBr_6$ solar cells.[19] The lifetime of 1.4 µs we measured by transient absorption spectroscopy is an order of magnitude longer than typically observed from lead–halide perovskite thin films under similar fluences,[29] and is also longer than previously measured for methylammonium lead iodide/bromide single crystals with low trap density.[1] This microsecond lifetime is approaching that for upgraded metallurgical-grade multicrystalline-silicon used in solar cells.[30]

From the measured lifetime, we can calculate the carrier density under open-circuit conditions when the photon flux of the incident laser is equal that of 1 sun AM 1.5G illumination (4.7×10^{17} photons $s^{-1} cm^{-2}$). The details of these calculations are given in Section S3 in the Supporting Information. For our $Cs_2AgBiBr_6$ thin film, we calculated a steady-state carrier density of $2.2 \times 10^{16} cm^{-3}$. This is an order of magnitude higher than the steady-state carrier density of methylammonium lead iodide thin film at 295 K ($5.2 \times 10^{15} cm^{-3}$; calculations detailed in Section S3 in the Supporting Information), suggesting that $Cs_2AgBiBr_6$ can have low resistance to charge transport under illumination. We note that if we attempted to estimate the steady-state carrier density from our TRPL measurements of the same film, we would obtain a value of only $5.3 \times 10^{13} cm^{-3}$ and therefore significantly under-estimate the carrier density. This emphasizes the importance of our work in showing that the sub-bandgap PL decay does not represent the recombination of most photocarriers.

In conclusion, using transient absorption spectroscopy, we have found that the fundamental lifetime of $Cs_2AgBiBr_6$ thin film is 1.4 µs. Our results indicate that the transport properties in $Cs_2AgBiBr_6$ could support thicker active layers, which could lead to increased current densities and higher power conversion efficiencies through enhanced light absorption. Our work also provides new insights into the recombination dynamics of silver–bismuth double perovskites. We find that the weak PL is red-shifted to the optical bandgap and decays two orders of

magnitude faster than the ground state bleach measured on the same timescale. This is likely due to recombination via subgap states rather than across the indirect bandgap. We also find that the decay in PL matches the rise in an excited state that decays on a microsecond timescale. This opens up questions on the role of defects and their interactions with excitations on photocarrier decay. Future understanding of these phenomena could lead to improvements in this class of lead-free perovskites.

Experimental Section

Double Perovskite Single Crystal Synthesis: 1 mmol CsBr (99.9% Sigma Aldrich), 0.5 mmol AgBr, and 0.5 mmol $BiBr_3$ (≥98% Sigma Aldrich) were fully mixed in 6 mL HBr acid (47% EMPLURA) at 70 °C. After stirring for 1 h, the solution was cooled to room temperature and any precipitates were filtered out. The clear solution was then placed into a fridge (≈4 °C). Millimeter-sized single crystals were collected after 1 week via vacuum filtration, followed by washing in acetone. AgBr was prepared by adding $AgNO_3$ (99.85% Acros Organics) into water solution of KBr (molar ratio of 1:1). Light green precipitates were filtered and then dried in an oven. Similar procedures were used to synthesise $Cs_2AgBiCl_6$ crystals, except that >10 mL HCl acid (37% Sigma Aldrich) was necessary to fully dissolve a similar amount of CsCl (≥99% Sigma Aldrich), $AgNO_3$, and bismuth acetate (99% Alfa Aesar), due to the low solubility of AgCl.

$Cs_2AgBiBr_6$ Thin Film Synthesis: 1.2 mmol CsBr (99.9% Sigma Aldrich), 0.6 mmol AgBr (≥98% Sigma Aldrich), and 0.6 mmol $BiBr_3$ (≥98% Sigma Aldrich) were dissolved in 1 mL dimethyl sulfoxide (≥99.9% Sigma Aldrich) and mixed at 900 rpm at 130 °C inside a N_2-filled glovebox. Glass substrates were cleaned by ultrasonication in acetone and isopropanol for 15 min each, followed by 10 min O_2 plasma cleaning at 300 W (forward power) in a radio frequency (RF) plasma system. The substrates were subsequently taken into a N_2-filled glovebox and heated at 75 °C for at least 5 min. To deposit the films, the substrate was placed onto a vacuum-free chuck, and 50 µL solution immediately dropped onto the substrate while warm, before spinning at 2000 rpm for 40 s. These films were annealed over a range of temperatures from 150 to 300 °C for optimization, as detailed in Figure S5 in the Supporting Information. The films used for spectroscopic investigations were annealed at 250 °C.

Characterization: PDS is a highly sensitive surface averaged absorption measurement technique. For the measurements, a monochromatic pump light beam produced by the combination of a Light Support MKII 100 W Xenon arc source and a CVI DK240 monochromator was illuminated on the sample (a double perovskite single crystal held onto a quartz substrate using polystyrene or a double perovskite thin film on quartz), inclined perpendicular to the plane of the sample, which on absorption produced a thermal gradient near the sample surface via nonradiative relaxation-induced heating. This resulted in a refractive index gradient in the area surrounding the sample surface. This refractive index gradient was further enhanced by immersing the sample in a deflection medium comprising of an inert liquid FC-72 Fluorinert (3M Company) which had a high refractive index change per unit change in temperature. A fixed wavelength CW transverse laser probe beam, produced using a Qioptiq 670 nm fiber-coupled diode laser with temperature stabilizer for reduced beam pointing noise, was passed through the thermal gradient in front of the sample producing a deflection proportional to the absorbed light at that particular wavelength, which was detected by a differentially amplified quadrant photodiode and a Stanford Research SR830 lock-in amplifier combination. Scanning through different wavelengths gave the complete absorption spectrum.

Time-resolved photoluminescence measurements using an intensified charge-coupled device camera were measured with an Andor iStar DH740 CCI-010 system connected to a grating spectrometer (Andor SR303i). Excitation was made at 400 nm wavelength from a frequency-doubled Ti:Sapphire laser (Spectra Physics Solstice) with

a wavelength of 800 nm, repetition rate of 1 kHz and pulse length of ≈100 fs. For measurements of the single crystals, the gate width was 1.5 ns and step 4 ns. The exposure time was 0.3 s and slit width 200 μm for $Cs_2AgBiBr_6$ and 300 μm for $Cs_2AgBiCl_6$. For the $Cs_2AgBiBr_6$ thin film, the gate step and widths were 5 ns, with an exposure time of 1 s, gain of 150–200, and slit size of 400 μm.

For the transient absorption measurements, a Ti:Sapphire amplifier system (Spectra Physics Solstice), operating at 1 kHz and generating 90 fs pulses, was split to produce the pump and probe beams. The broad band probe beam (500–800 nm wavelength) was generated in a home-built noncollinear optical parametric amplifier. The pulsed excitation was provided by the second harmonic of the Ti:Sapphire, at 400 nm, for short-time measurements (200 fs–1 ns). For long time delay measurements (1 ns–100 μs), the third harmonic of a Nd:YVO4 laser (AOT-YVO-25QSPX, Advanced Optical Technologies), at 355 nm wavelength, with electronically controlled delay was used. The pump and probe beams were overlapped on the sample adjacent to a reference probe beam. This reference was used to account for any shot-to-shot variation in transmission. The beams were focused into an imaging spectrometer (Andor, Shamrock SR 303i) and detected using a pair of linear image sensors (Hamamatsu, G11608) driven and read out at the full laser repetition rate by a custom-built board from Stresing Entwicklungsburo. A mechanical/electronic chopper was used to create "pump-on" and "pump-off" periods during all measurements, with lock-in detection enabling separation of the signals and calculation of the differential transmission, $\Delta T/T$. To match the magnitude of the spectra measured on the short and long timescales, the short-time spectra were linearly scaled, such that the 0.1–1 ns spectrum had the same maximum $\Delta T/T$ value as for the 1–2 ns spectrum.

Photoluminescence quantum efficiency measurements were taken inside an integrating sphere according to a previously reported method.[31] Excitation was from a 405 nm wavelength continuous diode laser. The power was measured using a silicon photodetector (Thorlabs S130c). The photon flux inside the integrating sphere was measured using an Andor iDus DU490A CCD detector in air at room temperature.

UV–vis spectrophotometry measurements were performed using a PerkinElmer Lambda 750 UV-Visible spectrometer inside an integrating sphere. The reflectance and transmittance of the $Cs_2AgBiBr_6$ thin film on glass were separately measured. The instrument was calibrated to 0% and 100% reflectance/transmittance prior to measuring the sample. The measurements were taken from 1300 to 400 nm wavelength with an interval of 2 nm. The absorption coefficient was calculated using a previously reported method,[32,33] and using the measured thickness of the thin film (524 nm, from Dektak profilometry).

X-ray photoemission spectroscopy measurements were taken on $Cs_2AgBiBr_6$ thin films deposited on indium tin oxide (ITO) coated glass, and on $Cs_2AgBiCl_6$ single crystals. A monochromatic Al K$_{\alpha1}$ X-ray source ($h\nu = 1486.6$ eV) was used, with a SPECS PHOIBOS 150 electron energy analyser. The total energy resolution was 0.50 eV. The binding energy was calibrated using a polycrystalline Ag foil placed in electrical contact with the samples, which simultaneously helped to avoid charging effects during the measurement.

Supporting Information

Supporting Information is available from the Wiley Online Library or from the author. Raw data available from https://doi.org/10.17863/CAM.22601.

Acknowledgements

Conflict of Interest

The authors declare no conflict of interest.

Keywords

[1] D. Shi, V. Adinolfi, R. Comin, M. Yuan, E. Alarousu, A. Buin, Y. Chen, S. Hoogland, A. Rothenberger, K. Katsiev, Y. Losovyj, X. Zhang, P. A. Dowben, O. F. Mohammed, E. H. Sargent, O. M. Bakr, *Science* **2015**, *347*, 519.

[2] C. Wehrenfennig, G. E. Eperon, M. B. Johnston, H. J. Snaith, L. M. Herz, *Adv. Mater.* **2014**, *26*, 1584.

[3] S. de Wolf, J. Holovsky, S.-J. Moon, P. Löper, B. Niesen, M. Ledinsky, F. Haug, J. Yum, C. Ballif, *J. Phys. Chem. Lett.* **2014**, *5*, 1035.

[4] J. M. Richter, M. Abdi-Jalebi, A. Sadhanala, M. Tabachnyk, J. P. H. Rivett, L. M. Pazos-Outón, K. C. Gödel, M. Price, F. Deschler, R. H. Friend, *Nat. Commun.* **2016**, *7*, 13941.

[5] NREL Efficiency Chart, 2017. UREL, https://www.nrel.gov/pv/ (accessed: April 2018).

[6] N. Wang, L. Cheng, R. Ge, S. Zhang, Y. Miao, W. Zou, C. Yi, Y. Sun, Y. Cao, R. Yang, Y. Wei, Q. Guo, Y. Ke, M. Yu, Y. Jin, Y. Liu, Q. Ding, D. Di, L. Yang, G. Xing, H. Tian, C. Jin, F. Gao, R. H. Friend, J. Wang, W. Huang, *Nat. Photonics* **2016**, *10*, 699.

[7] R. L. Z. Hoye, L. C. Lee, R. C. Kurchin, T. N. Huq, K. H. L. Zhang, M. Sponseller, L. Nienhaus, R. E. Brandt, J. Jean, J. A. Polizzotti, A. Kursumović, M. G. Bawendi, V. Bulović, V. Stevanović, T. Buonassisi, J. L. MacManus-Driscoll, *Adv. Mater.* **2017**, *29*, 1702176.

[8] R. L. Z. Hoye, P. Schulz, L. T. Schelhas, A. M. Holder, K. H. Stone, J. D. Perkins, D. Vigil-Fowler, S. Siol, D. O. Scanlon, A. Zakutayev, A. Walsh, I. C. Smith, B. C. Melot, R. C. Kurchin, Y. Wang, J. Shi, F. C. Marques, J. J. Berry, W. Tumas, S. Lany, V. Stevanović, M. F. Toney, T. Buonassisi, *Chem. Mater.* **2017**, *29*, 1964.

[9] A. M. Ganose, C. N. Savory, D. O. Scanlon, *Chem. Commun.* **2017**, *53*, 20.

[10] C. N. Savory, A. Walsh, D. O. Scanlon, *ACS Energy Lett.* **2016**, *1*, 949.

[11] Z. Xiao, W. Meng, D. B. Mitzi, Y. Yan, *J. Phys. Chem. Lett.* **2016**, *7*, 3903.

[12] A. H. Slavney, L. Leppert, D. Bartesaghi, A. Gold-Parker, M. F. Toney, T. J. Savenije, J. B. Neaton, H. I. Karunadasa, *J. Am. Chem. Soc.* **2017**, *139*, 5015.

[13] K. Z. Du, W. Meng, X. Wang, Y. Yan, D. B. Mitzi, *Angew. Chem., Int. Ed.* **2017**, *56*, 8158; *Angew. Chem.* **2017**, *129*, 8270.

[14] R. Jaramillo, M.-J. Sher, B. K. Ofori-Okai, V. Steinmann, C. Yang, K. Hartman, K. A. Nelson, A. M. Lindenberg, R. G. Gordon, T. Buonassisi, *J. Appl. Phys.* **2016**, *119*, 35101.

[15] R. E. Brandt, J. R. Poindexter, P. Gorai, R. C. Kurchin, R. L. Z. Hoye, L. Nienhaus, M. W. B. Wilson, J. A. Polizzotti, R. Sereika, R. Žaltauskas, L. C. Lee, J. L. MacManus-Driscoll, M. Bawendi, V. Stevanović, T. Buonassisi, *Chem. Mater.* **2017**, *29*, 4667.

[16] A. Polizzotti, A. Faghaninia, J. R. Poindexter, L. Nienhaus, V. Steinmann, R. L. Z. Hoye, A. Felten, A. Deyine, N. M. Mangan, J. P. Correa-Baena, S. S. Shin, S. Jaffer, M. G. Bawendi, C. Lo, T. Buonassisi, *J. Phys. Chem. Lett.* **2017**, *8*, 3661.

[17] Z. Zhao, F. Gu, Y. Li, W. Sun, S. Ye, H. Rao, Z. Liu, Z. Bian, C. Huang, *Adv. Sci.* **2017**, *4*, 1700204.

[18] A. H. Slavney, T. Hu, A. M. Lindenberg, H. I. Karunadasa, *J. Am. Chem. Soc.* **2016**, *138*, 2138.

[19] E. Greul, M. L. Petrus, A. Binek, P. Docampo, T. Bein, *J. Mater. Chem. A* **2017**, *5*, 19972.

[20] G. Volonakis, M. R. Filip, A. A. Haghighirad, N. Sakai, B. Wenger, H. J. Snaith, F. Giustino, *J. Phys. Chem. Lett.* **2016**, *7*, 1254.

[21] F. Wei, Z. Deng, S. Sun, F. Zhang, D. M. Evans, G. Kieslich, S. Tominaka, M. A. Carpenter, J. Zhang, P. D. Bristowe, A. K. Cheetham, *Chem. Mater.* **2017**, *29*, 1089.

[22] W. Meng, X. Wang, Z. Xiao, J. Wang, D. B. Mitzi, Y. Yan, *J. Phys. Chem. Lett.* **2017**, *8*, 2999.

[23] E. Greul, M. L. Petrus, A. Binek, P. Docampo, T. Bein, *J. Mater. Chem. A* **2017**, *5*, 19972.

[24] W. Pan, H. Wu, J. Luo, Z. Deng, C. Ge, C. Chen, X. Jiang, W. Yin, G. Niu, L. Zhu, L. Yin, Y. Zhou, Q. Xie, X. Ke, *Nat. Photonics* **2017**, *11*, 726.

[25] D. Bartesaghi, A. H. Slavney, M. C. Gélvez-Rueda, B. A. Connor, F. C. Grozema, H. I. Karunadasa, T. J. Savenije, *J. Phys. Chem. C* **2018**, *122*, 4809.

[26] Z. Xiao, W. Meng, J. Wang, Y. Yan, *ChemSusChem* **2016**, *9*, 2628.

[27] M. R. Filip, S. Hillman, A. A. Haghighirad, H. J. Snaith, F. Giustino, *J. Phys. Chem. Lett.* **2016**, *7*, 2579.

[28] E. T. McClure, M. R. Ball, W. Windl, P. M. Woodward, *Chem. Mater.* **2016**, *28*, 1348.

[29] S. D. Stranks, G. E. Eperon, G. Grancini, C. Menelaou, M. J. P. Alcocer, T. Leijtens, L. M. Herz, A. Petrozza, H. J. Snaith, *Science* **2013**, *342*, 341.

[30] J. A. Giesecke, B. Michl, F. Schindler, M. C. Schubert, W. Warta, *Energy Procedia* **2011**, *8*, 64.

[31] J. C. de Mello, H. F. Wittmann, R. H. Friend, *Adv. Mater.* **1997**, *9*, 230.

[32] R. L. Z. Hoye, R. E. Brandt, A. Osherov, V. Stevanovic, S. D. Stranks, M. W. B. Wilson, H. Kim, A. J. Akey, J. D. Perkins, R. C. Kurchin, J. R. Poindexter, E. N. Wang, M. G. Bawendi, V. Bulovic, *Chem. Eur. J.* **2016**, *22*, 2605.

[33] R. E. Brandt, R. C. Kurchin, R. L. Z. Hoye, J. R. Poindexter, M. W. B. Wilson, S. Sulekar, F. Lenahan, P. X. T. Yen, V. Stevanović, J. C. Nino, M. G. Bawendi, T. Buonassisi, *J. Phys. Chem. Lett.* **2015**, *6*, 4297.